Available online at www.sciencedirect.com

ScienceDirect

Energy Procedia 114 (2017) 2906 – 2920

Energy Procedia

13th International Conference on Greenhouse Gas Control Technologies, GHGT-13, 14-18 November 2016, Lausanne, Switzerland

Using pressure recovery at a depleted gas field to understand saline aquifer connectivity

Michelle Bentham[a], Gareth Williams[b], Hayley Vosper[a], Andrew Chadwick[a], John Williams[a] and Karen Kirk[a]

[a]*British Geological Survey, Environmental Science Centre, Keyworth, Nottingham, NG12 5GG*
[b]*British Geological Survey, The Lyell Centre, Research Avenue South, Edinburgh, EH14 4AP*

Abstract

A key uncertainty facing Carbon dioxide Capture and Storage (CCS) in saline aquifers is long term injectivity, which is primarily a function of the connected aquifer pore-volume within which formation brine can be displaced as the CO_2 is injected. Protracted injection testing to interrogate and prove the far-field connected pore-volume would increase the lead-in times for commissioning of storage sites and would significantly increase appraisal costs. Here we use natural gas production and subsequent reservoir recharge legacy data from the Esmond gas field in the UK sector of the southern North Sea to gain an understanding of the dynamic behaviour of the Bunter Sandstone, a major saline aquifer. Results suggest that Esmond has a connected pore volume of 1.83×10^{10} m^3, suitable for injecting CO_2 at a rate of up to 2 million tonnes per year for at least 55 years. 3D seismic data suggest that Esmond reservoir properties are likely to be replicated across the wider Bunter Sandstone aquifer, notably around the Endurance structure which was, until recently, proposed for a full-chain CCS project.

Peer-review under responsibility of the organizing committee of GHGT-13.

Keywords: CCS; CO_2 storage; CO_2 injectivity; storage capacity; flow simulation.

1. Introduction

The Triassic Bunter Sandstone Formation in the Southern North Sea provides the target storage reservoir for the now suspended White Rose Project. The storage site comprises a gently folded anticlinal structure known as

Peer-review under responsibility of the organizing committee of GHGT-13.
doi:10.1016/j.egypro.2017.03.1418

Endurance (previously termed 5/42, Fig 1), which has recently been evaluated for CO_2 storage through the drilling of an appraisal well by National Grid Carbon (NGC), the results of which demonstrated the suitability of the site for storage of CO_2 as proposed for the White Rose project [1]. Well testing indicated an average reservoir permeability of 270 mD, with no barriers or baffles to fluid flow within at least 1.3 km of the well. This radius is constrained by the duration of the test; capacities provided by the UK CO_2 Storage Evaluation Database (CO_2Stored) [2] indicate that much larger volumes of CO_2 could potentially be stored in the Endurance structure. If, however, the site were to be developed as a storage hub following successful implementation of the White Rose Project, the long term injectivity and dynamic capacity of the aquifer would need to be proven.

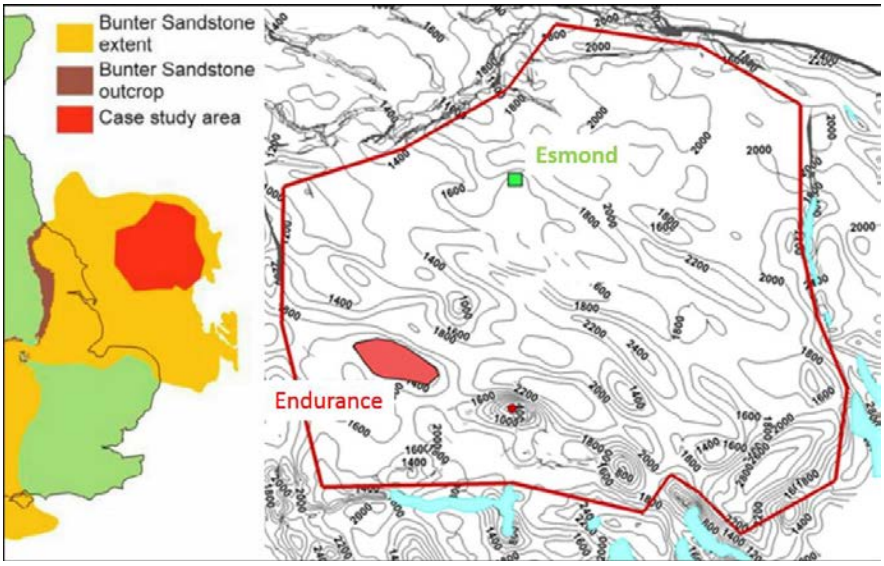

Fig. 1 Location of the Endurance (red) and the Esmond gas field (green). Contours show the depth to the top of the Bunter Sandstone Formation (metres)

In order to better understand the long-term injectivity of the Bunter reservoir at Endurance, pressure data from the nearby Esmond gas field (Fig. 2) has been used to calibrate dynamic models of the aquifer. The Esmond gas field is located at the culmination of a dome similar to that at Endurance (Fig 1). The field was produced by depletion drive, whereby gas is lifted to the surface driven by reservoir formation pressure, which is maintained by connected aquifer waters encroaching into the gas reservoir as the pressure drops during gas production. The invading aquifer water drives gas to the producing wells, improving recovery: this is indicative of extensive hydraulic communication within the aquifer. The degree to which water invades the reservoir depends on the size of the adjoining aquifer and the degree of communication between the aquifer and gas reservoir. If a gas reservoir is hydraulically connected to a larger aquifer, post-production reservoir pressures will progressively recover as water floods into the depleted gas field.

Gas production at the Esmond field began in 1985 with 8866 x 10^9 m^3 of gas (at STP) produced at the cessation of production in 1996. Measurements taken at the time of field abandonment show a significant reduction in reservoir pressure. In 2008 Esmond was considered for natural gas storage, and re-entered by a new appraisal well which indicated that the field had largely re-pressurised. Although the gas storage plans were subsequently abandoned, the pressure measurements provide a unique and rare post-production pressure dataset indicating connectivity of the reservoir to a significant aquifer volume.

Using fluid-flow simulations to history-match the observed pressure history of the Esmond Field, we estimate the size of the hydraulically-connected aquifer around Esmond and use this as an analogue for the likely aquifer volume surrounding the proposed Endurance storage site. This is followed by a qualitative comparison of seismic reflection

data over the two areas to assess whether there are any potential additional flow barriers around Endurance that might adversely affect pressure dissipation.

2. Background to the Esmond gas field

The Esmond field lies some 50 km to the NNE of the Endurance structure (Fig. 1) and, together with the neighboring Forbes and Gordon fields, makes up the Esmond gas complex. Bunter Sandstone thicknesses increase gradually from ~0 m north of Esmond, to ~400 m south of Endurance. At Esmond it comprises an upper sand (~6 m thick) and a lower sand (~90 m thick), separated by a ~7 m thick mudstone. Esmond produced around 8.5 x 10^9 standard cubic metres (sm^3) of gas (at standard conditions of 15°C and 1 atmosphere pressure) by 1995. It has been estimated that 93% of the gas was recovered, with 90% (around 7.6 x 10^9 sm^3) produced from the lower sand and around 5.75 x 10^8 sm^3 remaining in the reservoir [3]. Well-head pressure and production data [4] formed the basis for the history match described in this report (Fig.2).

An initial reservoir pressure of ~157 bars was measured at the top of the gas cap at the onset of production in 1985, and had reduced to ~10 bars at cessation of production 10 years later. A subsequent appraisal well 43/13a-5 was drilled in 2008. This showed that pressure in the upper sand remained depleted at around 10 bars, whereas reservoir pressure in the lower sand had recovered to ~120 bars at a depth of 1448 metres, around 80% of hydrostatic (Fig. 2). This indicates that the lower sand is laterally well-connected to the surrounding aquifer system but the upper sand is not, with the intra-reservoir mudstone acting as an effective short-term barrier to vertical water flow in the reservoir at least on production time scales.

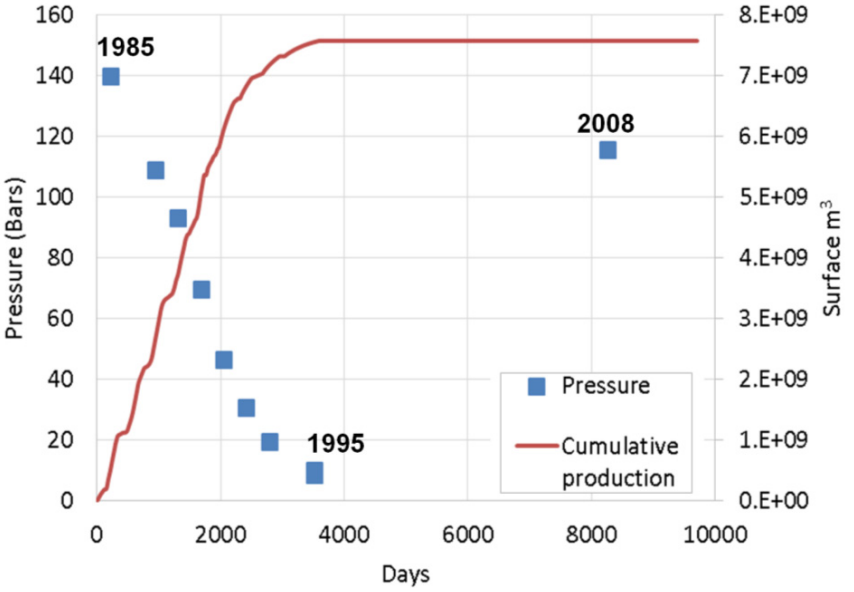

Fig. 2 Gas production (sm^3) and pressure history (bar) for the lower Bunter Sandstone reservoir in the Esmond field. The blue points show the pressure effect of gas extraction between 1985 and 1995 and subsequent pressure recovery by 2008. The red curve shows the cumulative gas production from the lower reservoir.

The good lateral flow connectivity in the lower Bunter Sandstone reservoir is consistent with interpreted seismic reflection data acquired over the Esmond field, which show that the reservoir is gently folded (by salt diapirism) but not affected by significant or pervasive faulting. Localised faults are present on the flanks of the folds and are locally associated with minor igneous intrusions (dykes), which could potentially form flow baffles. Localised small-scale faulting is likely to be characterised by sand/sand contacts, so fault-zone permeability should not be adversely affected

by shale entrainment processes, although mineral precipitation along fault surfaces cannot be ruled out. The presence of fault-related deformation bands (granulation seams) might also adversely affect permeability in the damage-zones close to any faults.

3. Methodology for assessing the Esmond aquifer

In order to determine the extent of the connected aquifer at Esmond, the pressure history was matched to the production and aquifer recharge data to infer the regional-scale flow properties and hydraulic capacity of the surrounding Bunter Sandstone aquifer. A suite of 1D axisymmetric numerical flow models was used to test a range of parameters including aquifer permeability, hydraulic connectivity and volumetric capacity. A more detailed 3D model was then built to refine the preferred solution, calibrated by seismic reflection and well datasets from the area, and also incorporating the peripheral pressure effects of production from the nearby Forbes field.

After establishing the dynamically-calibrated conceptual model for the Esmond-Forbes area, we carried out comparative qualitative assessment of the Bunter Sandstone at Esmond and Endurance using well and 3D seismic reflection data. The purpose was to examine the data for potential flow barriers (faults, salt walls, changes in diagenesis, facies changes and dyke intrusions), that might have an impact on the connected pore volume of the Bunter Sandstone and inferred injectivity.

3.1. Data

In addition to the gas production data, three 3D seismic reflection surveys were available, together with an additional high resolution 2D survey covering the Esmond and Forbes gas fields. Two of the 3D surveys, the proprietary Quads 42 & 43 survey and speculative Cavendish TQ3D survey, cover large areas to the NNW and SSE of the Esmond complex, while the Ravenspurn OBC survey provides coverage over the Endurance site (Fig. 3). Several regional 2D seismic lines were used to tie-in the 3D surveys. In addition, over 90 wells were used to constrain the interpretation, of which 53 had geophysical logs.

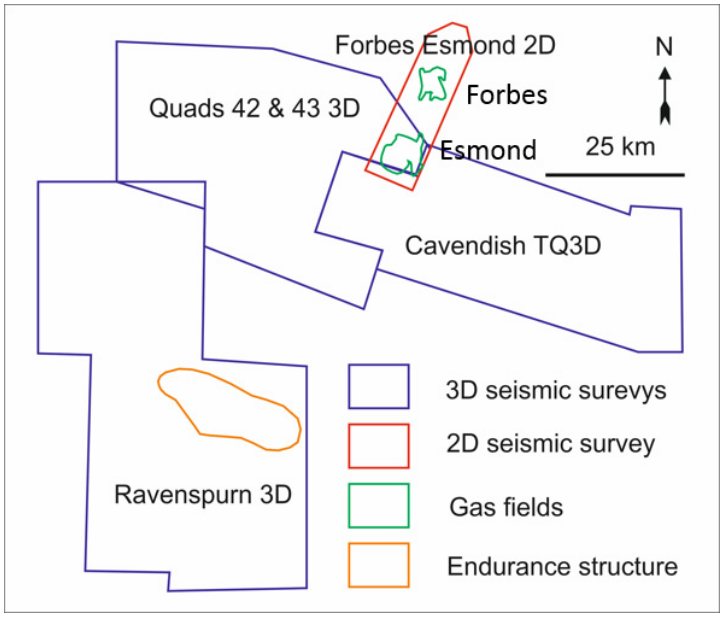

Fig. 3 Seismic survey data available for the study in the vicinity of the Forbes and Esmond gas fields and the Endurance structure.

3.2. Numerical models of Esmond

A series of simulations were run using the ECLIPSE 100 [5] reservoir simulator to history-match the observed pressure data (Fig. 2). In the initial modelling phase, simplified 1D axisymmetric models were constructed to investigate the effects of varying aquifer radius (analogous to connected aquifer volume), permeability, brine viscosity and compressibility, pore compressibility and gas-brine relative permeability on the modelled pressure curve. The results from these simulations were then used to parametrise a more detailed 3D reservoir model, incorporating the effects of reservoir topography and thickness to give more realistic pore volumes.

3.3. 1D axisymmetric flow models of Esmond

In the 1D axisymmetric models the reservoir was represented as a single layer 100 m thick, arranged with radial symmetry about an extraction borehole. The initial gas reserve was placed in the elements adjacent to the borehole at 100% saturation and the elements beyond filled with brine (Fig. 4).

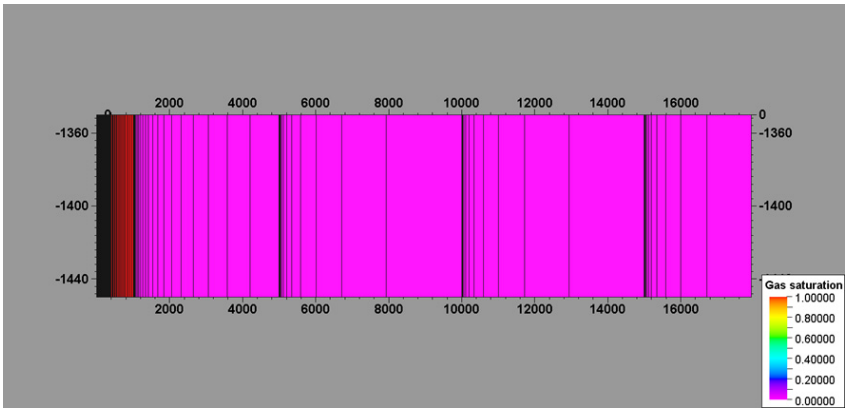

Fig. 4 1D simulation mesh showing the initial gas saturation (grid units in metres).

The total Gas In Place (GIP) was given by [3] as 290 x 10^9 cubic feet, or 8.21 x 10^9 m^3, at standard conditions of 15°C and 1 atmosphere pressure. Assuming an ideal gas, this translates to a gas volume of 5.94 x 10^7 m^3 at reservoir conditions. For a reservoir with a porosity of 0.18 and thickness of 100 m, this volume occupies a cylinder of radius 1025 m about the extraction borehole (Fig. 4). The mesh elements extend out to a radius of 59 km but the effective radial extent of the reservoir was adjusted by setting elements within the mesh to very low permeability. The simulations used black oil data tables computed for a mean reservoir temperature of 57°C and pressure of 157 bars. The fluid properties of brine were calculated using published correlations [6] while published densities and viscosities for pure methane [7] were used for the gas phase. Rock and fluid properties are summarised in Table 1.

Table 1 Rock and fluid property ranges used in the simulations.

Parameter	Minimum	Base case	Maximum
Porosity	0.18	0.18	0.18
Permeability (mD)	36	56	90
Pore compressibility (bar^{-1})	2.5 x 10^{-5}	5.0 x 10^{-5}	8.5 x 10^{-5}
Gas density ($kg.m^{-3}$)	98	98	98
Gas viscosity (cP)	0.016	0.016	0.016
Brine density ($kg.m^{-3}$)	1096	1096	1096
Brine viscosity (cP)	0.55	0.70	0.75
Brine compressibility (bar^{-1})	3.0 x 10^{-5}	3.5 x 10^{-5}	4.5 x 10^{-5}

3.4. 3D modelling

A 3D static geological model of the Bunter Sandstone aquifer incorporating the Esmond, Forbes and Gordon gas fields was built using PETREL. The Bunter Sandstone is compartmentalised into two hydraulically distinct units in this part of the Southern North Sea basin, the upper and lower sands (as discussed above), separated by the Solling Claystone which acts as a flow barrier on simulation timescales [8,9]. The reservoir model only included the thicker lower sandstone unit, from which 90% of the gas was produced. The North Dogger Fault Zone (NDFZ) forms the northern edge of the model [10], with arbitrary planar boundaries to the west, south and east. These represent no-flow boundaries in the simulations; however the total area of the 3D model is such that it greatly exceeds the radial extent of the connected aquifer calculated by the first phase of 1D axisymmetric model runs.

The resulting simulation grid comprised 242 x 189 x 45 cells in the I, J and K directions respectively (Fig. 5), giving average cell dimensions of 390 m (X) x 390 m (Y) x 2.5 m (Z). The model has a surface area of around 5.5 x 10^9 km^2 and a total pore volume of around 1.0 x 10^{11} m^3. The vertical layering was built upwards from the base of the reservoir, with proportional thickness changes to maintain an equal number of layers across the model. A minimum cell thickness of 1 m was specified, causing the upper layers to progressively pinch-out beneath the Hardegsen Disconformity at the northern margin of the grid. The horizontal cell dimensions represent a compromise between topographic resolution and simulation run-times, but are considered adequate for modelling the effects of regional fluid flow.

3.5. Rock and fluid properties and initial conditions

Initial rock and fluid properties were derived from a combination of measured and published data [3, 8, 11] (Tables 2 and 3). Mean porosity and permeability measurements taken from available core plug data from 23 wells in the Bunter Sandstone are shown in Table 2 [11]. A value of 0.18 (midway between the geometric and arithmetic mean values) is used in all the simulation runs described below. The lower bound value of 36 mD approximates the geometric mean of the measured horizontal permeability, while an upper bound value of 120 mD lies between the geometric and arithmetic mean values.

The 3D model was initialised using the pressure field generated from an equilibration run. A gas-water contact (GWC) 1451 m below mean sea level in the Esmond field and 1756 m in the adjacent Forbes field was used to define the gas in place (GIP), at a residual brine saturation of 0.15. This resulted in an initial GIP of around 9.0 x 10^9 sm^3 or 3.2 x 10^{11} sft^3 in Esmond prior to gas production. The resulting model was run to stability over 5000 years to generate a stable pressure field with fluids in equilibrium. This generated a gas buoyancy pressure of just over 7 bars at the top of the Esmond gas-cap (comparable to the value of 8 bars recorded in field appraisal wells).

Table 2 Mean porosity and horizontal (H) and vertical (V) permeability (mD) data, taken from 23 wells that penetrate the Bunter Sandstone in the Southern North Sea. K_A denotes permeability to air, whilst K_L is the Klinkenberg corrected liquid permeability [11].

	Porosity (%)	KH_A (mD)	KV_A (mD)	KH_L (mD)	KV_L (mD)
Arithmetic	19	446	294	483	415
Harmonic	14	0.6	0.5	0.5	0.3
Geometric	17	41	16	34	26

Table 3 Key reservoir parameters used in the simulations [3, 8, 11].

	Esmond Field	Forbes Field
Residual brine saturation	0.15	0.15
Reservoir temperature (C)	57	63
Initial reservoir pressure (bar)	157	193
Depth to gas-water contact (m)	1451	1756
Gas in place (sm^3)	8.97 x 10^9	1.7 x 10^9

4. Flow simulation results

The 1D axisymmetric models provided a convenient abstraction to the 3D problem allowing for rapid parameter testing and sensitivity analysis. Given the uniform porosity and thickness assumed in the 1D models, their connected pore-volume is directly proportional to the square of aquifer radius. The 1D models show that the magnitude of pressure draw-down during gas extraction is largely determined by the intrinsic permeability of the aquifer. The magnitude of the pressure recovery during aquifer re-charge is a function of aquifer radius, a proxy for connected pore-volume. By systematically varying permeability and the radial extent of the axisymmetric model, it was found that a closed reservoir of radius of 17 km and permeability 56 mD gave a good fit to the measured pressure data (Fig. 5a, red curve). However, it is noted that it was also possible to match the data using smaller aquifer radii with 'leaky' boundary conditions. Leaky boundary models require significant brine flux across the boundary in order for the model to satisfy the pressure constraints. Pore compressibility also influenced aquifer recovery, with the best fit to the pressure measurements given by values in the range 4.0–5.5 x 10^{-5} bar^{-1}.

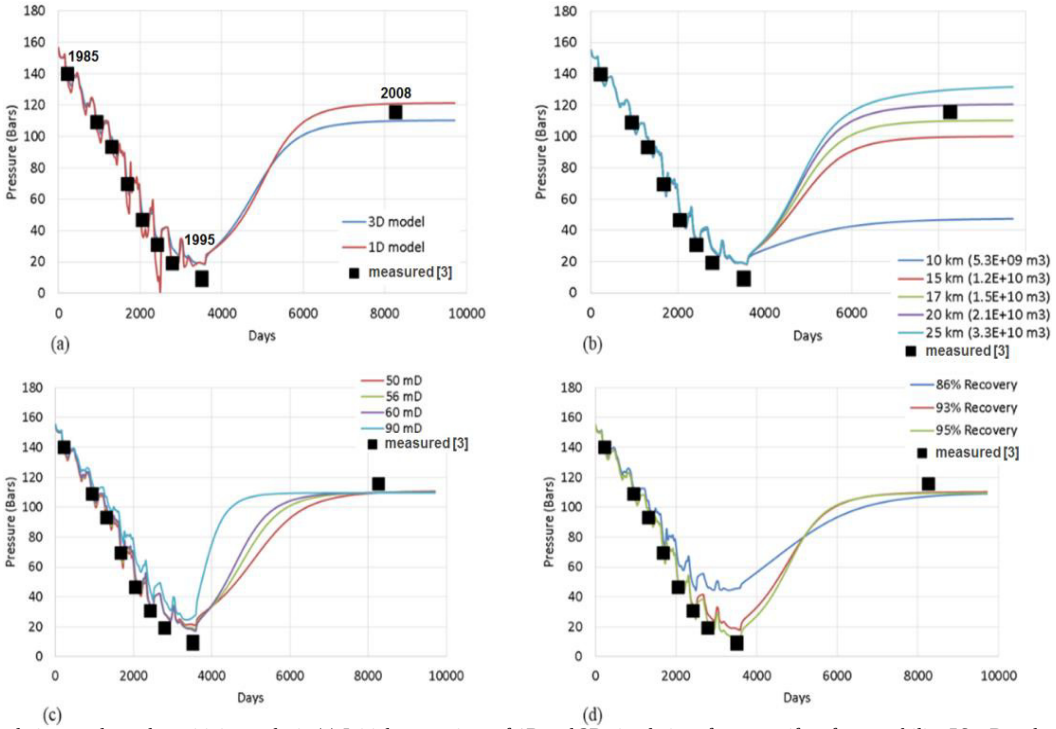

Fig. 4 Flow simulation results and sensitivity analysis (a) Initial comparison of 1D and 3D simulations for an aquifer of permeability 56 mD and radius 17 km. The small discrepancy in pressure recovery between the two models reflects minor differences in the 1D and 3D connected pore-volumes. (b) Comparison of 3D simulations illustrating the effect of varying connected aquifer radius (pore-volume) on the pressure response. (c) Comparison of 3D simulations illustrating the effect of varying aquifer permeability on pressure response, for a fixed aquifer radius of 17 km. (d) Effect of percentage gas recovery on the modelled pressure response. Best fits are achieved at >90% recovery.

The 3D flow simulations also make use of a radially symmetric approximation to bulk pore-volume, with active cells assigned within a circle of known radius (Fig. 6). The connected extent of the modelled 3D aquifer is henceforth referred to in terms of aquifer radius, analogous to the 1D axisymmetric modelling. Initial parameterisation of the 3D model using the properties established by the 1D modelling yields comparable results (Fig. 5a). The variable reservoir thickness in the 3D model introduces a small change in total pore-volume compared to the 1D case but the discrepancies are sufficiently small to permit an acceptable match between the calculated pressures for the 1D and 3D simulations (Fig. 5a). Note that for simplicity one production well was modelled in the 3D case whereas in reality a number of wells were used to produce the field.

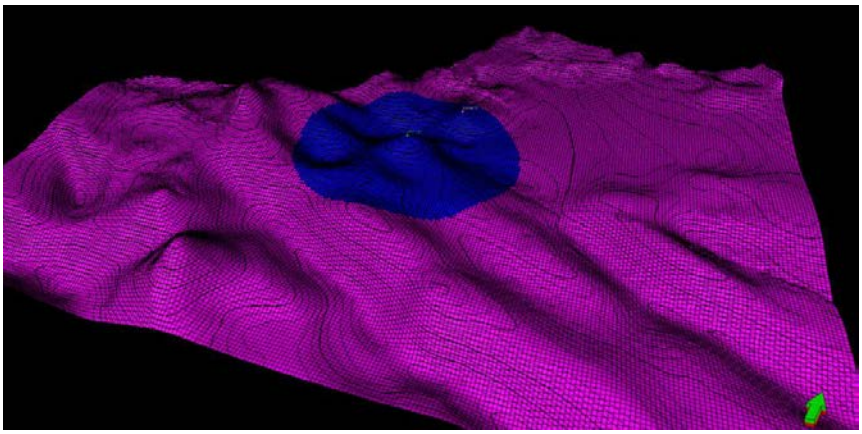

Fig. 5 The connected pore-volume of the 3D numerical flow model is set by making the model cells within a given radius active (blue), with inactive cells outside it (pink).

4.1 Sensitivity to permeability and aquifer radius (connected pore-volume)

Sensitivity of the pressure response to aquifer pore-volume was tested by progressively increasing the radial extent of active cells in the 3D simulations (Fig. 5b). As in the 1D case, permeabilities in the 50 – 60 mD range are required to match the observed pressure drawdown in the vicinity of the production well (Fig. 5c). After further extensive parameter testing is was concluded that a connected aquifer of radius of 18.5 km and permeability of 56 mD provides the preferred fit to the data (Fig. 6, red curve).

4.2 Sensitivity to Gas in Place (GIP)

Pre-production GIP was estimated at around 8.21 x 10^9 m^3 (or 290 x 10^9 ft^3) [3], which approximately corresponds to a GWC of 1451 m in the reservoir model. This gives around 93% gas production with the published production figures [4]. By varying the height of the GWC in the 3D model slightly it was possible to test the pressure response of the reservoir to the total GIP (or, more specifically, the percentage gas depletion). Not surprisingly end-production pressures are very sensitive to the (rather small) amount of gas remaining in the reservoir (Fig. 5d). It proved necessary to produce over 90 % of GIP to match the pressure drawdown observed by 1995, with the ‘best fit’ model producing 95% of GIP (Fig. 5d).

4.3 Impact of Forbes Field gas production

The Esmond Field is part of a larger gas complex, together with the nearby Forbes Field 12 km to the north-east, and the Gordon Field some 35 km to the south-east. If there were pressure communication between the two fields, gas production from Forbes would likely impact on the pressure recovery at Esmond, given their close proximity. The results of simulating the effect of Forbes production (Fig. 6) indicate that it might well reduce the amount of water available to recharge Esmond, with a small but noticeable negative impact on pressure recovery. In order to regain the quality of modelled fit, it was necessary to increase the effective aquifer radius to 20 km to match the observed pressure recovery at Esmond. In reality the Esmond and Forbes fields are separated by two zones of igneous dyke intrusion, which are likely form barriers to fluid flow. These were not included in the flow simulation so the ‘Forbes effect’ might be less significant than modelled.

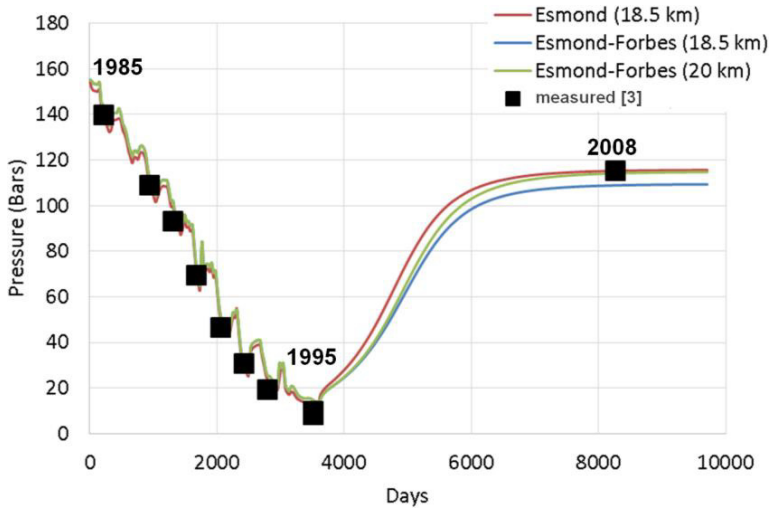

Fig. 6. Comparison of 3D simulations assessing the effect of gas production from the nearby Forbes Field on the pressure response at Esmond.

4.4 Summary of 3D model simulations

The 3D model simulations largely confirm the 1D axisymmetric modelling, with the best fit to the measured data given by a model with an aquifer radius of 18.5 km, a connected pore volume of 1.8 x 10^{10} m^3 and a total production of 95% of GIP (Fig. 6, red curve). If gas production from the Forbes Field is included in the modelling, the connected aquifer radius is increased to 20 km to match the observed pressure recovery at Esmond (Fig. 6, green curve). It is notable that this notional aquifer boundary does correspond to some real geological features at similar distance, notably to the north-west and north-east of Esmond, where the North Dogger Fault Zone is likely to form an effective flow barrier.

5. Evidence for aquifer connectivity in the region surrounding the Esmond gas field and the Endurance structure

Evidence from previous studies of the Bunter Sandstone aquifer in this region [11, 12, 13] suggests that there are a number of geological features that might inhibit the movement of fluids over short timescales (i.e. during CO_2 injection) and affect the dynamic storage capacity of the aquifer. Here we set out the results of a qualitative comparative study of existing seismic and well data in the areas of Esmond and Endurance which identified five geological features that could potentially act as barriers to flow (Fig. 7):

- Regional fault zones
- Salt walls
- Crestal faulting associated with halokinesis (movement of underlying salt layers)
- Dyke intrusion
- Potential diagenetic cementation (identified as a polarity reversal on seismic data).

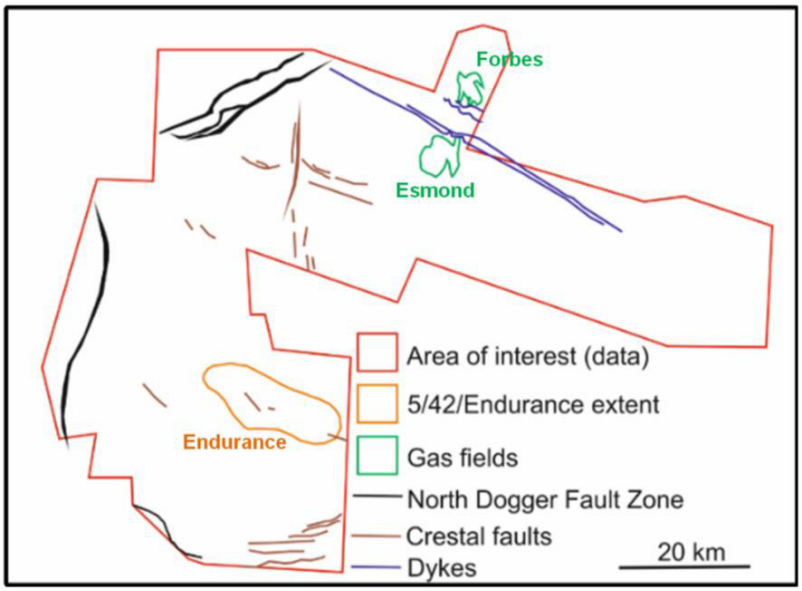

Fig. 7 Regional fault zones, crestal faulting and intrusive dykes, as potential barriers to fluid flow in the Bunter Sandstone identified in this study.

5.1. Regional flow barriers

The North Dogger and Dowsing fault zones [12] are major fault systems running across the north-west corner of Quadrants 42 & 43. They lie some 25 km north and west of Esmond and 30 - 40 km to the north and west of Endurance (Figs. 7, 8) and are structurally complex with large and variable displacements. The top Bunter Sandstone seismic reflector cannot be reliably traced across the zone of faulting, where locally the Bunter Sandstone is completely offset by the fault. It is likely that stratigraphic juxtaposition of the Bunter Sandstone against the Zechstein (an evaporite and mudstone sequence), Bunter Shale or Haisborough Groups (composed of evaporite, shale and dolomite) across the North Dogger Fault Zone will form a potential barrier to fluid flow.

In addition, an east-trending linear belt of large salt walls cuts the Bunter Sandstone some 30 km to the east and south of Endurance, with more salt features 60 km due east of Esmond. Salt is effectively impermeable to reservoir fluids, and so is likely to form a barrier to flow on the southern and eastern boundary of the study area.

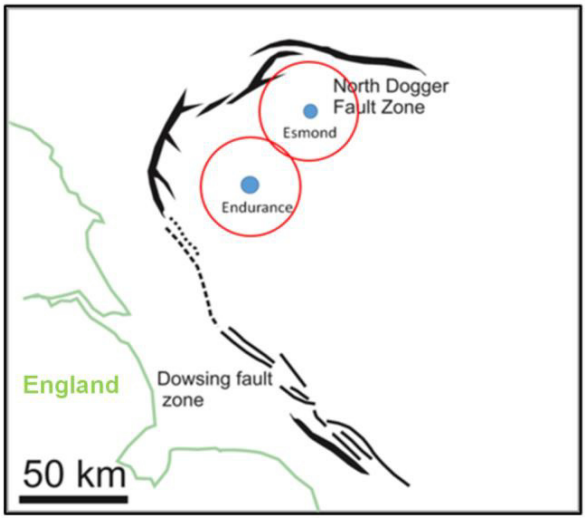

Fig. 5 Potential regional flow barriers showing the major North Dogger and Dowsing fault zones (adapted from [10]). Circles with a radius of 20 km from the centroids of the Esmond field and Endurance structure are shown in red.

Crestal faulting

Movement of the underlying Zechstein evaporites has folded the Bunter Sandstone into a series of broad domes, which provide the structural traps for the Esmond, Forbes and Gordon gas fields and the closure for the Endurance structure. Extension of the sedimentary cover above these structures is often accommodated by mainly rather small normal faults on the crest and flanks of the domes (Fig. 68). Most of the mapped faults show little or no seismically resolvable offset at the top Bunter Sandstone surface, although they frequently displace overlying strata (Fig. 8b). Small throws at reservoir level tend to self-juxtapose the reservoir sandstones. There is no data available regarding the potential of these faults to compartmentalise the Bunter Sandstone, but they should not adversely affect fluid flow in the absence of well-developed shale smearing, fault gouge or pervasive deformation bands.

Only one of the mapped crestal faults fully offsets the Bunter Sandstone (Fig. 8, Fault F1), in this case juxtaposing the Haisborough Group in the hanging wall of the fault with the Bunter Shale in the footwall. Both these formations largely comprise low permeability rocks that will likely impede cross-fault fluid flow. This fault is not regionally extensive. It is orientated north-south and has a length of around 13 km, forming a small graben with a smaller fault (Fig. 8, Fault F2) to the west at the top of the dome, 20 km to the west of the Esmond Field.

There is evidence from the seismic data of some minor faulting at the top Bunter Sandstone in the vicinity of the Endurance structure, although data quality is insufficient to map fault offsets in detail. Crestal faulting is also present in the Bunter Sandstone along the axis of a dome 13 km south of the Endurance structure. Here the Bunter Sandstone is partially offset at top reservoir level. It is concluded that crestal faulting is unlikely to form major barriers to flow in the study area but in some cases might act as baffles.

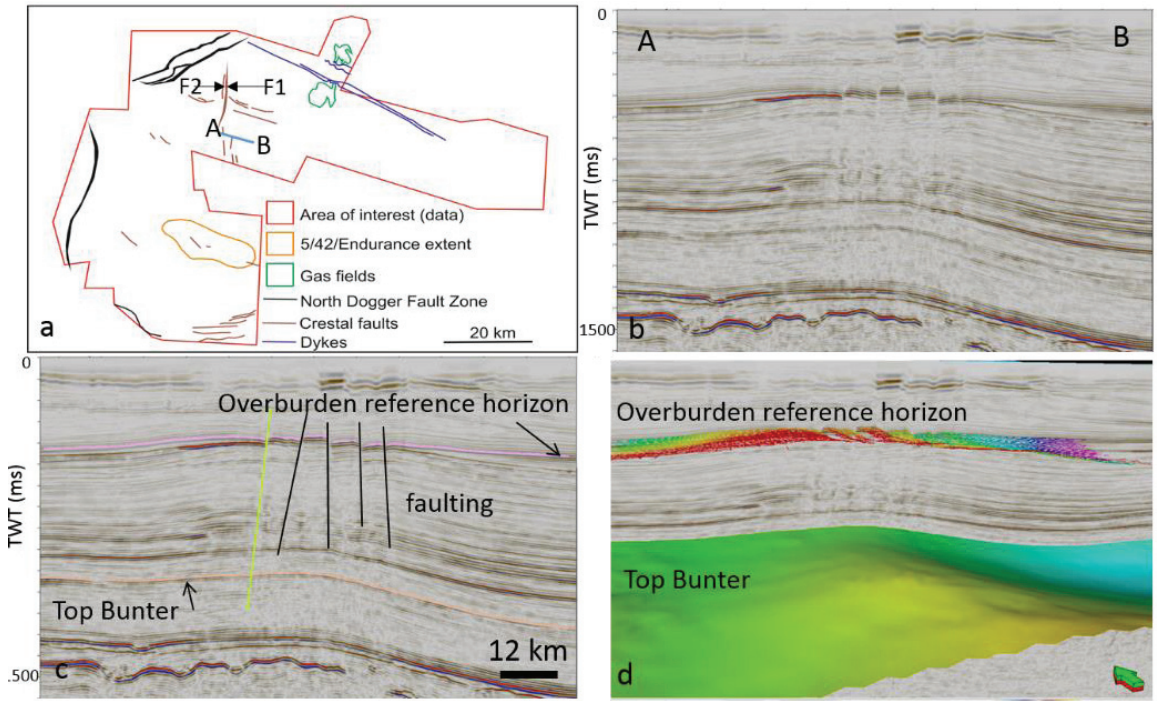

Fig. 6 Examples of minor crestal faulting mapped in the Esmond Field and Endurance structure study area. The location of the seismic line illustrated is shown in panel a. Panels b and c show the un-interpreted and interpreted seismic data, respectively. Faults can be seen in the overburden above the Bunter Sandstone reservoir, of which only one (green) is seismically detectable at reservoir level. Panel d shows the top Bunter Sandstone surface, as a cut-away in the 3D seismic data, which displays no visible offset beneath these faults.

Dykes

Igneous dykes are formed when magma is intruded into fractures in the host rock formation, forming vertical or steeply dipping roughly planar sheets of poorly-permeable crystalline rock. Evidence of Cenozoic dyke emplacement in the Southern North Sea has been observed on seismic and magnetic data [14, 15]. Features interpreted as dykes have been mapped on seismic data between the Esmond and Forbes fields, cutting the Bunter Sandstone less than a kilometre from the north-eastern boundary of the Esmond Field and extending NNW–SSE across the study area (Fig.7). There are no similar features visible on seismic data in the vicinity of the Endurance field however. Igneous intrusions in the Faroe-Shetland Basin have been interpreted to act as both barriers and pathways for fluid flow [16], but there is no evidence as to their impact in the study area.

Seismic polarity reversal

The top Bunter Sandstone was interpreted on seismic data as a positive acoustic impedance contrast across most of the study area. However, a local phase reversal in the seismic wavelet was observed in the vicinity of the Endurance structure (Fig. 9) and also in patches north of Esmond. This phenomenon was described by [1] in their site assessment of the Endurance structure. Wells within the zone of phase reversal record a bulk formation porosity in excess of 25%, whereas wells on the periphery of the phase reversal show a reduced porosity of <10%. Diagenetic cementation is thought to be the cause of this porosity reduction. Cementation could potentially reduce aquifer porosity and permeability to the west of the Endurance structure, but there is no evidence to show how far this low-porosity zone extends to the north and west. The average porosity of the Bunter Sandstone reservoir in the Esmond gas complex, also outside the zone of phase reversal, was recorded as 23–24 % [11].

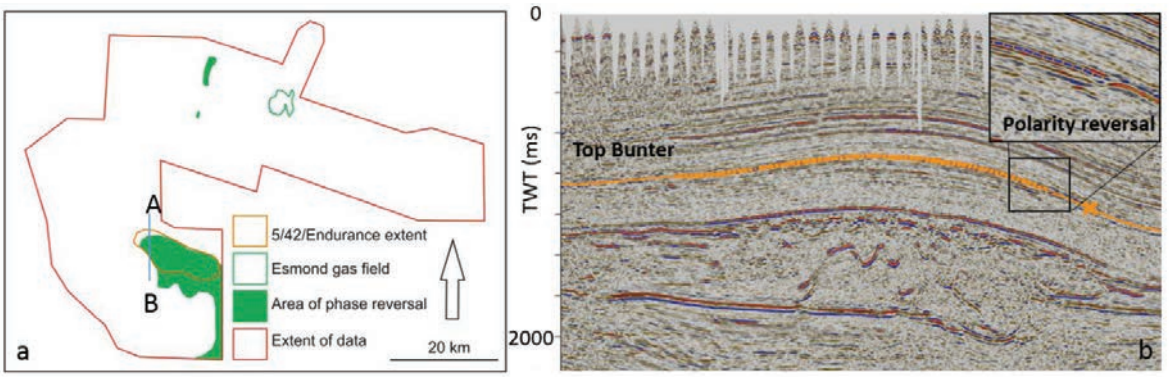

Fig. 7 a) Area of seismic polarity reversal (green) at the top Bunter Sandstone reflection in the vicinity of the Endurance Field (b) an interpreted seismic profile showing the top Bunter Sandstone surface (yellow) illustrating phase reversal (inset). Data courtesy of Schlumberger.

5.2. Summary of qualitative evaluation of potential flow barriers

The principal geological and structural features interpreted from seismic data and their potential impact on fluid flow are summarised (Table 4). It is likely that the main baffles to fluid flow through the Bunter Sandstone are formed by the large North Dogger and Dowsing fault zones to the north and west and the salt walls towards the southern and eastern limits of the area. Other features such as crestal faults and igneous dykes are considered to be of lesser or localised significance. The impact of the diagenetic features associated with seismic polarity reversal is still uncertain however.

Table 4 Summary of geological and structural features which might reduce aquifer connectivity in the vicinity of the Esmond field and Endurance structure.

Structure	Minimum distance from the Esmond Gas Field	Minimum distance from the Endurance structure	Likelihood of acting as a flow barrier	Is the feature likely to have a regional or local affect?
North Dogger Fault Zone	25 km	22 km	High	Regional
Crestal faulting (minor offset)	20 km	0 km	Unknown	Local
Crestal fault (top BNS fully offset)	20 km	N/A	High	Local
Dykes	<1 km	N/A	Unknown	Regional
Diagenetic cement (phase reversal)	Unknown	0 km	Unknown	Local
Salt walls	60 km	25 km	Low (too distal to have an impact on recharge at Esmond), may have an impact on injection at Endurance depending on scale.	Regional

6. Discussion

The study has shown that the aquifer properties evidenced around the Esmond gas field are likely to be replicated across the Bunter Sandstone aquifer more generally, and at the Endurance structure in particular. Assuming a connected storage volume with a boundary at 18.5 km radius, the Esmond structure has a connected pore-volume of 1.83×10^{10} m^3. In terms of static capacity this pore-volume could theoretically hold around 1.28×10^4 million tonnes of CO_2 (assuming full utilization of the pore-space and an *in situ* density of 700 kg m^3). Taking commonly assumed

storage efficiencies in the range 2 – 4% the connected volume would have a realistic static capacity of 260 to 510 million tonnes of CO_2.

A key aspect however is the rate at which the connected volume could receive CO_2 without damaging the storage system. A simple analytical radial model [17] of pressure increase during CO_2 injection was applied to both the Esmond Field (the focus of this modelling study) and the Endurance Structure (the proposed storage site for the White Rose CCS Project). Pressure increase was calculated for injection into the Bunter Sandstone aquifer with a closed radial boundary 18.5 km from the injection well. The results suggest that injecting at rates of ≤2 Mt per year will optimise the volume of CO_2 stored in the reservoir (≥100 Mt over a period of 100 years), without exceeding the fracture pressure of the overlying caprock close to the injection well (Table 5). However if higher injection rates were deployed (>2 Mt/year) then the rapid early increase in fluid pressure following the onset of injection could potentially fracture caprock in the vicinity of the wellbore after only a few years. This analysis does not, however, take into account any pressure amelioration because of brine flow through a seabed outcrop in the vicinity of Endurance [11].

Table 5 Calculated CO_2 storage capacity of the Esmond gas field and Endurance structure for different injection rates, assuming that the caprock will fracture at 80% of lithostatic pressure. The values represent lower bounds and are derived based on fluid over-pressures measured at a radial distance of 1 m from the injection well.

Injection rate (x10^6 tons / year)	Esmond gas field (x10^6 tons)	Endurance structure (x10^6 tons)
1	93	>100
2	80	~110
5	5	10

7. Conclusion

Long term injectivity, a key uncertainty facing CO_2 storage in saline aquifers, has been assessed for the Bunter Sandstone Formation in the vicinity of the Esmond gas field and, by analogy, for the nearby Endurance structure. This study has used gas production and subsequent reservoir recharge data to gain an understanding of the dynamic behaviour of the wider regional Bunter Sandstone saline aquifer and its suitability for large-scale CO_2 injection.

A series of reservoir simulations was run to history-match production pressure data and subsequent pressure recovery observed at the Esmond field. This has the established regional-scale flow properties and hydraulic connectivity of the surrounding Bunter Sandstone aquifer. A suite of 1D axisymmetric numerical flow models were used to test a range of parameters including aquifer permeability, hydraulic connectivity and volumetric capacity. A more detailed 3D flow model was then built to refine the preferred solution, calibrated by seismic reflection and well datasets from the area, and also incorporating the peripheral pressure effects of production from the nearby Forbes field. To history-match the observed pressure recovery at Esmond the model required a connected aquifer of 18.5 to 20 km radius with a bulk mean permeability of between 50 and 60 mD, dependent on model sensitivities.

Qualitative examination of 3D seismic reflection data around the Esmond gas field, with evaluation of potential geological flow barriers, is consistent with the dynamic modelling results, and indicates that the reservoir is connected to an aquifer volume with a radius of at least 18.5 km.

Comparative assessment of 3D seismic data in the vicinity of Esmond and Endurance indicate that the latter is likely to be more favorable for CO_2 storage due a thicker reservoir and lack of (seismically resolvable) flow barriers in the vicinity. This provides a degree of confidence that the Bunter Sandstone saline aquifer surrounding the Endurance structure would have had a sufficiently well-connected pore-volume to allow the injection of CO_2 for the duration of the White Rose project at a rate of up to 2 Mt of CO_2 per year. Uncertainty remains however on the significance of diagenetic features in the Bunter Sandstone which might significantly reduce dynamic capacity. Further work is needed to fully understand these effects.

Acknowledgements

The Authors would like to thank Dr Ward Goldthorpe and The Crown Estate for funding this work, and Tom Mallows for useful comments and insight. We would also like to acknowledge Schlumberger (Graham Milne) who

provided seismic data for analysis. This paper is published with the permission of the Executive Director of the British Geological Survey (NERC).

References

[1] Furnival S, Wright S, Dingwall S, Bailey P, Brown A, Morrison D, De Silva R. 2014.Subsurface Characterisation of a Saline Aquifer Cited for Commercial Scale CO_2 Disposal. Energy procedia, 63, p4926–4936.
[2] Bentham M, Mallows T, Lowndes J, Green A 2014. CO_2 Storage Evaluation Database (CO_2 Stored). The UK's online storage atlas. Energy Procedia, 63, p5103–5113. www.co2stored.co.uk
[3] Schwarz, 2009, Esmond Gas Storage Project UK North Sea Block 43/13a UK North Sea
Block 43/13a (www.encoreoil.co.uk/assets_cm/files/PDF/encore_gas_storage_presentation_
from_oct_2009_ps.pdf)
[4]https://itportal.decc.gov.uk/information/wells/pprs/Well_production_offshore_gas_fields/well_gas_production_by_year_/well_gas_production_by_year.htm
[5] Schlumberger, 2011. Eclipse Technical Description 2011.1
[6] Batzle, M. L., Wang, Z. Seismic properties of pore fluids. *Geophysics* 1992: ***57****; 1396–1408.*
[7] NIST. Thermophysical Properties of Fluid Systems. *http://webbook.nist.gov/chemistry/fluid/*
[8] Bifani R. 1986 Esmond Gas Complex. Habitat of Paleozoic Gas in N. W. Europe. Geological Society, Special Publication. 23. p209-221
[9] Ketter FJ. 1991. The Esmond, Forbes and Gordon Fields, Blocks 43/8a, 43/13a, 43/15a, 43/20a, UK North Sea. In: Abbotts, I.L. (ed.) United Kingdom Oil and Gas Fields, 25 Years Commemorative Volume. Geological Society, London, Memoir 14, p.425–432.
[10] Griffiths PA, Allen MR, Craig J, Fitches WR, Whittington RJ. Distinction between fault and salt control of Mesozoic sedimentation on the southern margin of the Mid-North Sea High. Geological Society, London, Special Publications 1995, v. 91, p.145-159
[11] Noy DJ, Holloway S, Chadwick RA., Williams J.D.O., Hannis SA, Lahann RW. 2012. Modelling large-scale carbon dioxide injection into the Bunter Sandstone in the UK Southern North Sea. International Journal of Greenhouse Gas Control, 9, p.220–233.
[12] Bentham MS, Green A, Gammer D. 2013. The Occurrence of Faults in the Bunter Sandstone Formation of the UK Sector of the Southern North Sea and the Potential Impact on Storage Capacity. Energy prccedia. 37, p.5107-5109.
[13] Brook M, Shaw K, Vincent C, Holloway S. 2003. GESTCO case study 2a-1: Storage potential of the Bunter Sandstone in the UK sector of the Southern North Sea and the adjacent onshore area of eastern England. British Geological Survey Commissioned Report, CR/03/154N.
[14] Underhill JR. 2009. Role of intrusion-induced salt mobility in controlling the formation of the enigmatic 'Silverpit Crater', UK Southern North Sea. Petroleum Geoscience. 15. P.197-216.
[15] Wall M, Cartwright J, Davies R, McGrandle. 2009. 3D seismic imaging of a Tertiary Dyke Swarm in the Southern North Sea. Basin Research. 22. P.181-194.
[16] Rateau R., Schofield N, Smith N. 2013. The potential role of igneous intrusions on hydrocarbon migration. West of Shetland. Petroleum Geoscience, 18, p.259-272.
[17] Mathias S.A, Hardisty PE, Trudell MR, Zimmerman RW. 2008. Approximate Solutions for Pressure Buildup During CO_2 Injection in Brine Aquifers. Transport in Porous Media 79, doi:10.1007/s11242-008-9316-7, p.265–284.